

Enhanced weak superconductivity in trigonal γ -PtBi₂

J. Zabala, V. F. Correa,* F. J. Castro, and P. Pedrazzini

Centro Atómico Bariloche and Instituto Balseiro, CNEA,
CONICET and U. N. de Cuyo, 8400 San Carlos de Bariloche, Argentina

(Dated: April 10, 2024)

Electrical resistivity experiments show superconductivity at $T_c = 1.1$ K in a high-quality single crystal of trigonal γ -PtBi₂, with an enhanced critical magnetic field $\mu_0 H_{c2}(0) \gtrsim 1.5$ Tesla and a low critical current-density $J_c(0) \approx 40$ A/cm² at $H = 0$. Both T_c and $H_{c2}(0)$ are the highest reported values for stoichiometric bulk samples at ambient pressure. We found a weak H_{c2} anisotropy with $\Gamma = H_{c2}^{ab}/H_{c2}^c < 1$, which is unusual among superconductors. Under a magnetic field, the superconducting transition becomes broader and asymmetric. Along with the low critical currents, this observation suggests an inhomogeneous superconducting state. In fact, no trace of superconductivity is observed through field-cooling–zero-field-cooling magnetization experiments.

PACS numbers: 74.25.Fy, 74.62.Bf, 73.43.Qt

I. INTRODUCTION

Topological matter (TM) is arguably one of the current hot topics in condensed-matter physics. Unlike traditional states of matter, where the physical properties are ultimately set by inter-particle interactions, in the TM, the key role is played by symmetry. Although originally restricted to a few specific systems, the number of topological material candidates has grown immensely over the last few years [1]. Electronic topological phases range from insulators to superconductors showing singular surface states that may differ substantially from bulk states [2, 3]. The concurrence of different topological phases on a single system would be a major finding aimed at getting further insight into the TM physics.

PtBi₂ is a unique material. It crystallizes into four different polymorphs [4]. Two of these, cubic β -PtBi₂ and trigonal γ -PtBi₂, are topological semimetal candidates. Both phases are metastable at room temperature; therefore, a thermal-quenching procedure is performed during crystal growth to retain these phases [5]. Despite this, high-quality single crystals are obtained with a residual resistivity $\rho_0 < 1 \mu\Omega$ cm and residual resistivity ratio RRR = $\rho(300\text{K})/\rho(0)$ of several hundred [6, 7]. The semimetallic character is confirmed by the low carrier density $n_c \sim 10^{20}$ cm⁻³ [6, 8]. Nonetheless, the carrier mobility $\mu > 1$ m²V⁻¹s⁻¹ is very high [6, 8] due to a superposition of a large mean free path $l_0 > 1 \mu\text{m}$ [8, 9] and a low effective mass [10, 11].

Cubic β -PtBi₂ shows one of the largest non-saturating transverse magnetoresistances among semimetals, $\text{MR} = (R(H) - R(0))/R(0) = 1.1 \times 10^5$ at temperature $T = 1.8$ K and magnetic field $\mu_0 H = 33$ T [8]. This behavior is ascribed to nearly compensated electrons and holes. Hall effect measurements and a quadratic MR confirm this scenario [8]. However, the MR becomes linear at high fields, a behavior that is claimed to be associated with

Dirac-like cones in the band structure [8]. Angle-resolved photoemission spectroscopy (ARPES) experiments along with density functional theory (DFT) show the existence of Dirac points close to the Fermi surface confirming β -PtBi₂ is a 3D Dirac semimetal [12, 13].

Trigonal γ -PtBi₂ also shows a semimetallic behavior [14] with a large magnetoresistance $\text{MR} = 230$ at $T = 2$ K and $\mu_0 H = 9$ T [11]. The MR displays an intricate non-saturating sub-quadratic field dependence greatly dependent on the field direction. At some specific angles, the MR is linear [11, 15]. The presence of open orbits [15] and/or Dirac surface states [16] and/or triply degenerate point fermions [11] are among the possible mechanisms to explain this behavior. In any case, carrier compensation does not seem to be the primary source for the large MR.

Superconductivity (SC) was reported in the PtBi₂ system several decades ago, with a sub-K value $T_c = 0.15$ K [17]. Recently, γ -PtBi₂ bulk single crystals were confirmed to be superconducting by means of electrical resistivity measurements, showing a $T_c = 0.6$ K and a low critical field $\mu_0 H_{c2}(0) = 60$ mT [5]. The associated superconducting transition is rather broad, $\Delta T_c \sim 0.2$ K. Rh-doping produces higher critical temperatures that reach $T_c = 2.75$ K in Pt_{0.65}Rh_{0.35}Bi₂, despite the introduction of substitutional disorder. In these samples, the transition remains broad and it is considerably dependent on the electrical current [5]. Robust SC, with $0.3 \text{ K} \leq T_c \leq 0.4$ K, has been also observed in γ -PtBi₂ thin flakes with anisotropic critical fields reaching $\mu_0 H_{c2}(0) \sim 0.3$ T [18]. The analysis of this anisotropy suggested that SC is 2D rather than surface SC. On the other hand, detailed DFT calculations predict a type-I Weyl semimetal band structure due to a broken inversion symmetry and strong spin-orbit coupling. Were it confirmed, γ -PtBi₂ would be the first type-I Weyl semimetal with superconducting properties at ambient pressure [18].

Both β and γ polymorphs show pressure-induced SC with a critical temperature $T_c \sim 2$ K, which remains almost unchanged up to 50 GPa. Pressure is detrimental to both the RRR and the MR while no trace of a pressure-

*Electronic address: victor.correa@cab.cnea.gov.ar

induced structural transition is detected [19, 20]. The onset of SC is accompanied by an abrupt increase of the carrier concentration and a sudden drop of the mobilities in β -PtBi₂, while the electron-hole balance still holds [19]. In γ -PtBi₂, a sign change of the Hall coefficient occurs exactly at the pressure onset of SC [20].

Local enhancement of SC is observed in point-contact spectroscopy experiments on γ -PtBi₂, reaching $T_c = 3.5$ K and $\mu_0 H_{c2}(0) = 3$ T. The origin of such effect seems to be a combination of local pressure and a change in the electron local density of states induced by the point contact [21]. More recently, two further stunning results have been disclosed in this phase. Scanning tunneling microscopy (STM) experiments detect superconducting gaps as large as 20 meV that are robust against a magnetic fields of several Tesla and a temperature of up to 5 K [22]. On the other hand, ARPES experiments combined with *ab-initio* calculations identify topological surface Fermi arcs that become superconducting at $T \sim 10$ K [23]. Both results are dependent on the preparation and type of sample surfaces.

This collection of results suggests that an outstanding type of superconductivity nucleates in γ -PtBi₂, with no conclusive reported evidence supporting a 3D bulk state in the undoped material. Additionally, a detailed study of the dependence of the SC state on the quality of bulk samples is still missing. In this work we contribute to this issue by reporting our first findings based on electrical transport results on a high-quality single crystal of γ -PtBi₂. We detect a superconducting state with a doubling of the critical temperature, $T_c = 1.1$ K, almost an order of magnitude enhancement of the critical field $\mu_0 H_{c2} \gtrsim 1.5$ T with a weak anisotropy, while still observing a large suppression of SC by a low electrical current in a bulk sample. To show our results we organize the manuscript as follows: Section II describes the crystal synthesis and characterization, Section III presents and discusses the $T < 2$ K electrical resistivity results with evidence of superconductivity, and finally, the conclusions are given in Section IV.

II. CRYSTAL SYNTHESIS, CHARACTERIZATION AND PHASE STABILITY

A. Single crystal growth and characterization

Single crystals of γ -PtBi₂ were grown by the self-flux technique. The initial mixture (Pt:Bi = 2.7 : 97.3; total mass = 9 g) of pure elements (Bi: > 99.999%; Pt: > 99.98%) was placed in an alumina Canfield Crucible Set which was then introduced in a quartz tube. The tube was evacuated and finally sealed after incorporating a small amount of Ar. This set-up was introduced into a resistive oven and kept at 950°C during 5 hours. Then it was rapidly cooled down (200°C/hour) to 360°C followed by a low speed ramp (8°C/day) to 296°C. At this temperature, the residual Bi-rich flux was removed

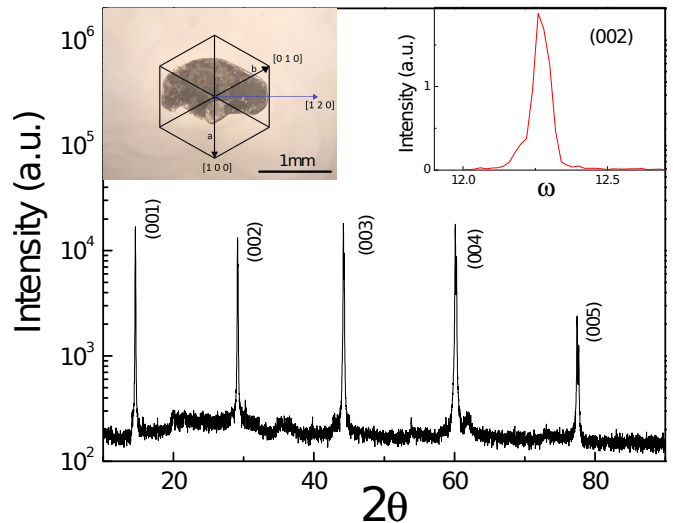


FIG. 1: X-ray diffraction $\theta - 2\theta$ scan corresponding to the $(00l)$ family planes of γ -PtBi₂ C1 crystal. Left inset: crystal image showing the direction of the crystal axes. Right inset: XRD ω -scan scan for the (002) peak.

using a centrifuge in a very rapid process, leading to the finding of platelet-like hexagonal-shaped single crystals.

Energy-dispersive x-ray spectroscopy (EDS) and x-ray diffraction (XRD) scans confirm the correct stoichiometry and trigonal structure of the samples. Figure 1 shows a $\theta - 2\theta$ XRD scan corresponding to the $(00l)$ family of planes. No spurious peaks other than $\text{Cu}-K_{\beta}$ reflections are observed. Lattice parameters $c = 6.157(8)$ Å and $a = 6.59(1)$ Å of the hexagonal conventional cell were calculated from $(00l)$ and $(h0h)$ reflections, in fair agreement with previously reported values [5, 11]. The rocking-curve (ω -scan) FWHM for the (002) peak is 0.06° , further supporting the good quality of the sample (right inset of Fig. 1).

The magnetic properties were measured in a SQUID magnetometer. γ -PtBi₂ is diamagnetic up to room temperature, as seen in Fig. 2. The magnetic susceptibility χ shows little temperature dependence with a small upturn below 50 K. There is some anisotropy between the c -axis ($H \parallel [001]$) and the in-plane ($H \perp [001]$) susceptibilities as already observed in Bi-deficient samples [6]. In our case, unlike what is reported in Ref. [6], $|\chi_c| < |\chi_{ab}|$. Different stoichiometries may explain this discrepancy.

A $1.4 \times 0.7 \times 0.2$ mm³ crystal labeled as C1 was separated for the magnetotransport experiments (see the left inset of Fig. 1). C1 was cut into a bar geometry using a thin razorblade. The longest length runs along the $[120]$ direction (see the left inset of Fig. 1). The sample was then successively exfoliated using scotch tape to a final thickness $e = 19$ μm along the c -axis. Electrical contacts for in-plane resistivity measurements were prepared using EPO-TEK H20E silver epoxy in a standard four-probe setup. The electrical current was applied along the $[120]$ direction. Resistance was measured either with a

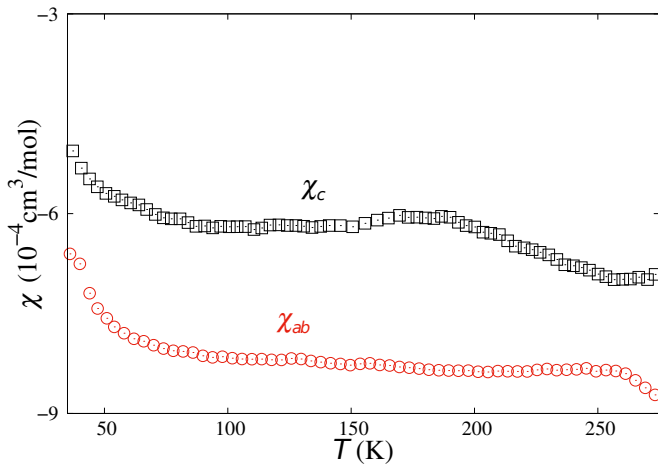


FIG. 2: Magnetic susceptibility $\chi(T)$ for the magnetic field ($\mu_0 H = 1$ T) applied along the c -axis (χ_c), or perpendicular to it (χ_{ab}).

LR-700 ac resistance bridge or in dc mode using a high-gain EM-A10 preamplifier with a HP34401A multimeter and a Keithley 220 current source.

Figure 3 shows the temperature dependence of the zero-field electrical resistivity from room temperature down to 2 K. A metallic behavior is observed. The extrapolated $\rho_0 \approx 0.13 \mu\Omega\text{cm}$ and $\text{RRR} \approx 320$ are comparable to those obtained from the best samples in the literature: $\rho_0 \sim 0.12 - 0.82 \mu\Omega\text{cm}$, $\text{RRR} \sim 162 - 640$, see Refs. [6, 11]. A prominent magnetoresistance, $\text{MR}(2\text{ K}, 9\text{ T}) = 41$, is also observed at low temperature in Fig. 3. At the lowest temperature, the MR is linear in field above $\mu_0 H = 10$ T (inset of Fig. 3). The MR is temperature independent below 4 K and it is drastically sup-

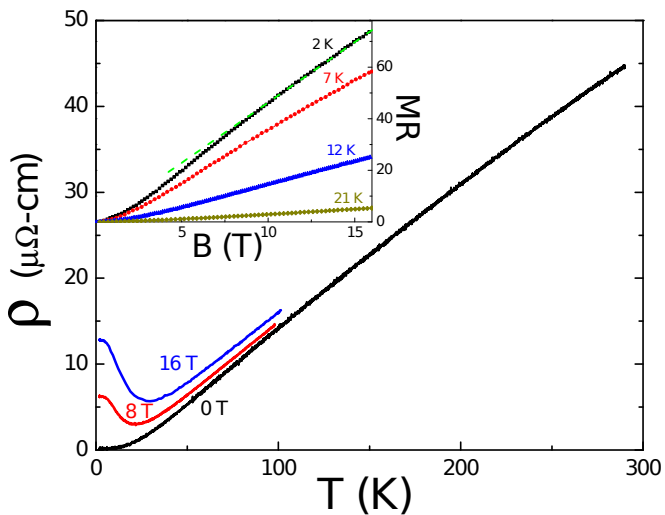


FIG. 3: Temperature dependence of the electrical resistivity at different magnetic fields. Inset: Magnetoresistance at different temperatures. The dashed line is a linear fit to the $\text{MR}(2\text{ K})$ data for $\mu_0 H > 10$ T.

pressed above 25 K. No Shubnikov-de Haas oscillations are observed for this $H \parallel [001]$ field direction. However, they emerge (not shown here) as the field is tilted away from this direction, in agreement with previous reports [18].

B. Phase stability

Since γ -phase is metastable at room temperature, a study of the phase stability under a thermal annealing process was performed using differential scanning calorimetry (DSC). A γ -PtBi₂ single crystal from the same batch was first heated from room temperature up to 450°C at 5°C/min. Then it was cooled down to room temperature again along 10 minutes, and finally the first ramp was repeated. The corresponding temperature variations of the heat flows are shown in Fig. 4 where phase transitions are assigned according to the Pt-Bi binary phase diagram [4].

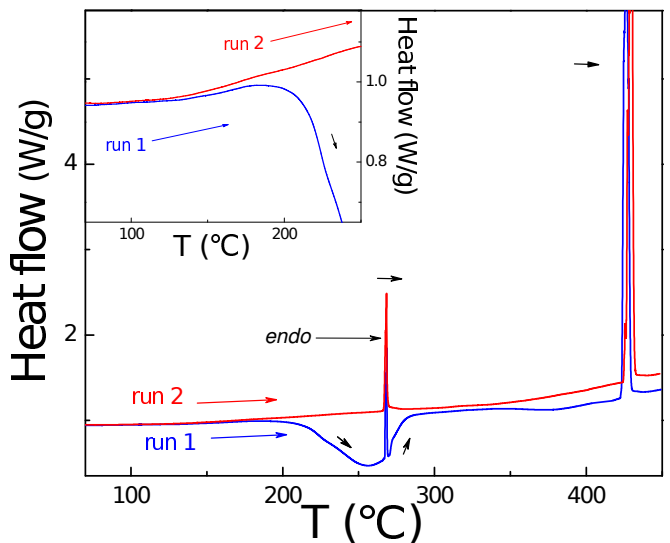


FIG. 4: Differential scanning calorimetry experiments in a γ -PtBi₂ single crystal, corresponding to two successive heating sweeps. Phase transitions are assigned according to the Pt-Bi binary phase diagram [4]. The inset depicts a magnified view of the lower temperature region, where the first and second heating runs split apart.

During the first run, a wide exothermic peak was observed above $T \approx 200^\circ\text{C}$ signaling a progressive transition from the metastable γ -phase to the stable orthorhombic α -phase. At $T = 270^\circ\text{C}$ a narrow endothermic peak is associated with the equilibrium transition from the α -phase to the β -phase. It is interesting to note that the broad exothermic peak extends above this $\alpha - \beta$ transformation, indicating that not all the metastable γ -phase has already re-transformed into the corresponding stable phase (either α or β). Another large endothermic peak observed around $T = 420^\circ\text{C}$ corresponds to the equilibrium $\beta - \gamma$ transition. During the second run, only

the equilibrium transitions were observed, implying that the intermediate cooling process was slow enough to allow the successive $\gamma - \beta - \alpha$ re-transformation. A zoom of the low temperature region (inset of Fig. 4) shows that the partial decomposition of the metastable γ -phase begins at temperatures as low as $T \sim 125^\circ\text{C}$ (where *run 1* and *run 2* curves split apart).

III. SUPERCONDUCTIVITY

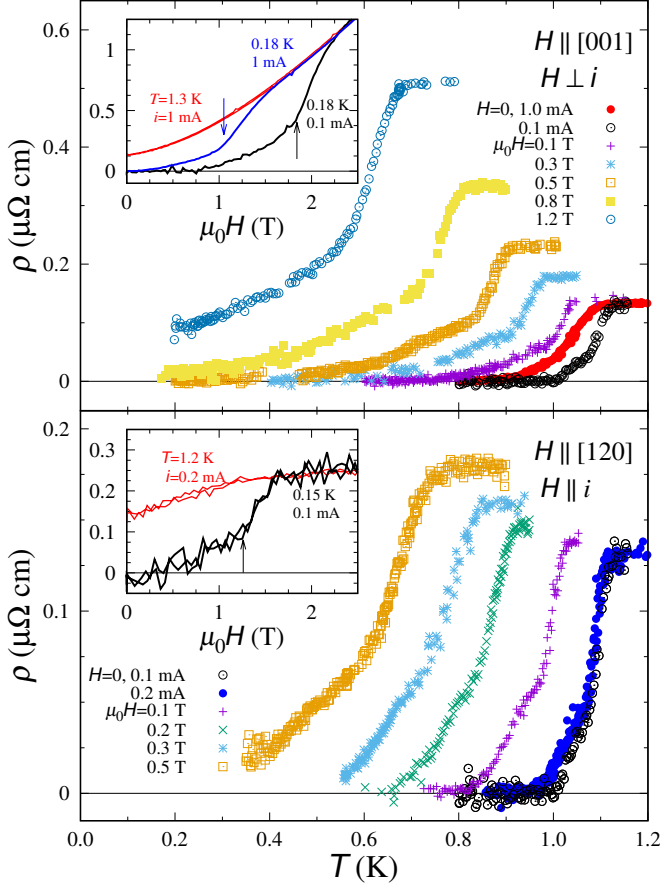


FIG. 5: Very-low-temperature dependence of the electrical resistivity at different magnetic fields and applied currents. A SC transition is observed at $T_c = 1.1\text{ K}$. Top panel: $\rho(T)$ at different fixed applied magnetic fields with ($\mathbf{H} \parallel [001]$) $\perp i$. Bottom panel: $\rho(T)$ with fixed ($\mathbf{H} \parallel [120]$) $\parallel i$. Insets: Magnetoresistance $\rho(H)$ at two different temperatures with the corres, above and below T_c . Arrows indicate the position of the onset of superconductivity at $T \lesssim 0.2\text{ K}$ measured either with current $i = 0.1\text{ mA}$ (\uparrow) or 1 mA (\downarrow). Onset fields are $\mu_0 H_{c2-on}^c \approx 2.2\text{ T}$ and $\mu_0 H_{c2-on}^{ab} \approx 1.5\text{ T}$.

Magnetotransport experiments were further extended to dilution fridge temperatures. In-plane resistivity results are displayed in Fig. 5 for two different field orientations. A superconducting transition is clearly observed, with critical temperature $T_c = 1.1\text{ K}$ (defined from the 50%–criterion $\rho(T_c) = 0.5\rho_N$, with $\rho_N = \rho(T \gtrsim T_c)$ the

normal state resistivity). The resistive transition is narrow, with a 10%–90% criterion width $\Delta T_c = 0.1\text{ K}$ for applied currents $i \leq 0.1\text{ mA}$. As the applied current increases, the transition broadens and shifts to lower temperatures, see the upper panel of Fig. 5 for a comparison between the $i = 0.1\text{ mA}$ and 1 mA measurements. Using a 50%–criterion, we estimate the critical current $i_c(T \rightarrow 0) \approx 3.5\text{ mA}$, yielding a critical current density as low as $J_c(0) \approx 40\text{ A/cm}^2$ assuming an homogeneous current distribution (see supplemental material [24] for a detailed current dependence of ρ). A similar strong current dependence was previously reported in the literature, although with a lower temperature onset for superconductivity and a broader resistive transition [5].

The suppression of SC by a magnetic field applied along the c -axis is shown in the top main panel of Fig. 5. A well defined superconducting transition is observed in $\rho(T)$ even for $\mu_0 H > 1\text{ T}$ although at such field a strict $R = 0$ state is not detected in the measured T -range. A stronger field suppression of $T_c(H)$ is detected when the field is applied parallel to the main surface of the sample $\mathbf{H} \parallel [120]$, see the lower main panel. These observations are further confirmed by the $\rho(H)$ data measured at $T \lesssim 0.2\text{ K}$ with $i = 0.1\text{ mA}$, depicted in both insets of Fig. 5. For $\mathbf{H} \parallel [120]$ ($\mathbf{H} \parallel [001]$) the data departs from $\rho \sim 0$ at roughly $\mu_0 H = 0.5\text{ T}$ (0.8 T), showing a broad transition into the normal state represented here by the $\rho(H)$ data at $T \sim 1.2\text{ K} > T_c$. Two further aspects of Fig. 5 are worth mentioning. First, the sizable MR observed in the normal state for $\mathbf{H} \perp i$ which is partially suppressed for $\mathbf{H} \parallel i$ (a small misalignment between the field and current directions could explain the surviving MR). Second, the distinctive structure in $\rho(T)$ across $T_c(H)$ showing a sharp drop and a field-dependent tail that extends towards low temperatures. Such resistive transitions resemble those in high- T_c superconductors that are usually associated to thermally-activated vortex motion [25]. In the low- T_c SC at hand, we tend to associate these structures to a broadening of the transition due to an inhomogeneous SC-state.

Figure 6 shows the $H - T$ phase diagram of our C1 crystal obtained from the $\rho(T)$ or $\rho(H)$ measurements of Fig. 5 and different applied currents. We first focus on the inset, where symbols represent the corresponding 50%–criterion critical values with H applied along the basal plane (squares), corresponding to H_{c2}^{ab} , or along the c -axis (circles), H_{c2}^c . The lowest temperature data point at $T \lesssim 0.2\text{ K}$ are determined from the 50% criterion applied to the $\rho(H)$ data of Fig. 5, yielding $\mu_0 H_{c2}^{ab} \approx 1.25\text{ T}$ and $\mu_0 H_{c2}^c \approx 1.85\text{ T}$. Assuming a minor role of surface superconductivity (H_{c3}) on the determination of H_{c2}^c , we obtain an anisotropy coefficient $\Gamma = H_{c2}^{ab}/H_{c2}^c \approx 0.7$ at the lowest T . The corresponding in-plane and out of plane coherence lengths are $\xi_{ab} = \sqrt{\phi_0/(2\pi H_{c2}^c)} \approx 13\text{ nm}$ and $\xi_c = \xi_{ab}/\Gamma \approx 19\text{ nm}$, where $\phi_0 = 2.07 \times 10^{-15}\text{ Wb}$ is the flux quantum. We note that these critical field values are much larger than previously reported for bulk γ -PtBi₂ crystals [5] and thin exfoliated flakes [18].

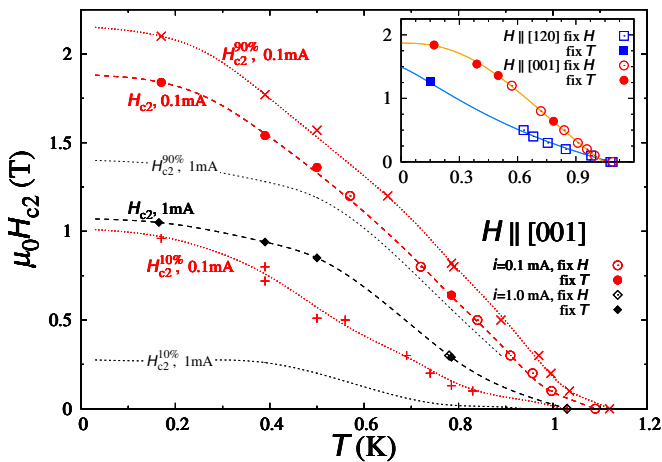


FIG. 6: Critical magnetic field $\mu_0 H_{c2}(T)$ for field applied along the c -axis defined with different criteria (10% – 50% – 90%) and two measuring applied currents: 0.1 mA (red data) and 1 mA (black data). The red-hatched area represents the width of the transition $\Delta T_c(H)$ as discussed in the main text. The discontinuous lines are guides to the eye. Inset: Critical magnetic field data for two different orientations, either along the c -axis, H_{c2}^c , or along the basal plane, H_{c2}^{ab} . Lines are fits of Eq. 1 to our data.

We now turn to the T -dependence of the critical fields. To do so, we first introduce a simple expression to describe $h \equiv H_{c2}(T)/H_{c2}(0)$ as a function of the reduced temperature $t = T/T_c$:

$$h(t) = \frac{1 - t^\alpha}{1 + t^\alpha}. \quad (1)$$

In this expression the exponent is usually taken to be $\alpha = 2$ [26], but we use α as a further fitting parameter in order to describe the large positive curvature of the data. The data for $H_{c2}^c(T)$ (red circles) can be closely reproduced in most of the studied T -range using parameters $\mu_0 H_{c2}(0) = 1.87(2)$ T, $T_c = 1.04(1)$ K and $\alpha = 2.49(6)$. The fit fails to describe the data in the low- H region ($\mu_0 H < 0.2$ T), where the convexity changes showing an upward curvature close to T_c . For $H_{c2}^{ab}(T)$, on the other hand, the convex behaviour extends in the broader range $0.6 \lesssim T/T_c < 1$. The corresponding fitting curve has parameters $\mu_0 H_{c2}(0) = 1.49(8)$ T, $T_c = 1.08(2)$ K and $\alpha = 1.2(1)$. In our measurements we find that $H_{c2}^{ab}(T) < H_{c2}^c(T)$ in the whole range of studied temperatures, supporting the $\Gamma < 1$ value calculated at the lowest measured temperature.

While the $H_{c2}(T)$ dependencies with changing convexity are ubiquitously encountered in chalcogenides [27, 28], iron arsenides [29], cuprates [30, 31] and other layered compounds, the inversion of the critical fields $H_{c2}^{ab}(T) < H_{c2}^c(T)$ we report here is an uncommon feature. In those compounds, a varying coupling among superconducting layers [32] and/or multiband effects [33] are usually claimed to be responsible for complex $H_{c2}(T)$ behaviours with a broad range of anisotropy values. In this case, the

anisotropy is rather weak but the apparent inversion of coherence length values $\xi_{ab} < \xi_c$ is both sizable and puzzling. Such $\Gamma < 1$ values have been previously reported in systems like UPd₂Al₃ thin films ($\Gamma = 0.85$) [34], UAu₂ at $p = 4.6$ GPa ($\Gamma = 0.9$) [35], and Lu₂Fe₃Si₅ single crystals ($\Gamma = 0.5$) [36]. The three of them are special cases: in both hexagonal U-compounds the SC-state emerges in antiferromagnetic (AFM) or nearly-AFM metals, while in the tetragonal Lu-compound 1-dimensional conducting chains are responsible for a larger conductivity along the c -axis, $\rho_{ab}/\rho_c \sim 4$ for $T \gtrsim T_c$. This is not the case for γ -PtBi₂, for which the magnetic response is weakly diamagnetic (see Fig. 2) and $\rho_{ab}/\rho_c \sim 0.01$ [9]. Despite this large transport anisotropy, we point out that a previous report on a bulk single crystal finds that the H_{c2} anisotropy is weak, with a value $\Gamma \sim 1.4$ [18, 37].

The simultaneous detection of enhanced T_c and H_{c2} values, together with a very low critical current J_c , could be related to the influence of inhomogeneities on the SC state (see also Ref. 37), despite the quoted high quality sample. The asymmetrical transition width in $\rho(T)$ at fixed H is a first evidence for the presence of such inhomogeneities. In the main panel of Fig. 6 we represent by a red hatched area the spread of the transition measured at low currents ($i = 0.1$ mA), limited by the 10% and 90%-criteria $H_{c2}^c(T)$. The 50%-criterion $H_{c2}^c(T)$ lies closer to $H_{c2}^{90\%}(T)$ and they both share a very similar T -dependence, while $H_{c2}^{10\%}(T)$ is further apart and shows a dependence that resembles that of $H_{c2}^{ab}(T)$, with a pronounced upward curvature in the range $0.5 \lesssim T/T_c < 1$. A larger current induces a strong suppression of the three H_{c2} lines, see the data measured at 1 mA in the main panel of Fig. 6 (black diamonds) showing that $H_{c2}(0)$ drops to almost half of its value at very low currents. As a further measure of the field suppression of the critical current, the quoted $J_c(0) \approx 40$ A/cm² for $H = 0$ drops down to $J_c(0) \approx 25$ A/cm² for $\mu_0 H = 0.3$ T. Note also the large broadening of the transition width ΔT_c at this measuring current, showing that a strict $R = 0$ state is not to be expected at fields $\mu_0 H \gtrsim 0.3$ T.

In a single crystal, local enhancement or reduction of the superconducting properties could be associated with local variations of composition, correlated defects, local strain, etc. In this sense, we point out that inhomogeneities in γ -PtBi₂ can readily appear due to the metastable character of this phase at room temperature. As shown in Fig. 4, sizable $\gamma \rightarrow \alpha$ retransformation starts at a moderate temperature $T \sim 125^\circ\text{C}$. The nucleation of very small amounts of α -phase could induce tensions in the bulk of γ -PtBi₂ and a corresponding microstructure of inhomogeneous material with different SC characteristics. In this sense, we point out that pressure applied to γ -PtBi₂ largely enhances both T_c and H_{c2} [20]. Alternatively, a surface state should be considered for the enhanced SC of our sample with low critical currents, in line with recent observations by STM and ARPES measurements [22, 23]. However, in this scenario we would expect a $\Gamma > 1$ anisotropy as evidenced by the critical

field ratio already discussed.

We finally point out that superconductivity is also observed in a second crystal C2 from the same batch and prepared following the same procedure as the one used for C1. Sample C2 displays a lower RRR ≈ 57 and its SC properties are depressed in comparison with sample C1: $T_c = 0.8$ K, $H_{c2}^{ab} \approx 0.55$ T, and a broader transition with $\Delta T_c(H = 0) \approx 0.4$ K. The onset temperature for SC, however, coincides in both samples at $T_c^{on} = 1.13$ K. The corresponding data are shown in the Supplemental Material [24]. Comparing both sets of results, in our samples increased quality (as measured by RRR) results in an enhancement of the superconducting parameters.

IV. CONCLUSIONS

We have provided evidence for an enhanced superconducting state in γ -PtBi₂ detected by means of in-plane electrical resistivity measurements performed on a high quality single crystal. The observed parameter $T_c = 1.1$ K is about twice the value previously reported in the bulk, while $\mu_0 H_{c2} \gtrsim 1.5$ T is at least 5

times larger. The critical current, on the other hand is rather small, leading us to suggest that this enhanced SC state is inhomogeneous within the bulk of our crystal. In fact, we cannot observe any trace of a superconducting state through field-cooling–zero-field-cooling magnetization experiments in a crystal from the same batch down to $T = 0.3$ K, practically discarding bulk superconductivity there. Our experiments cannot rule out the existence of intrinsic 2D superconductivity in very thin samples or a component of surface SC (in very clean surfaces) as it was proposed in previous works. The need for further macroscopic and spectroscopic studies in a more ample set of samples is thus evident.

Acknowledgements

The authors gratefully acknowledge N. Haberkorn and J.I. Facio for helpful discussions and a critic reading of the manuscript. Work partially supported by CONICET grant number PIP 2021-11220200101796CO, ANPCyT grant number PICT 2019-02396, Universidad Nacional de Cuyo (SIIP) grant number 06/C55T1.

-
- [1] M.G. Vergniory, B.J. Wieder, L. Elcoro, S.S.P. Parkin, C. Felser, B.A. Bernevig, and N. Regnault, All topological bands of all nonmagnetic stoichiometric materials, *Science* **376**, eabg9094 (2022).
- [2] X.-L. Qi and S.-C. Zhang, Topological insulators and superconductors, *Rev. Mod. Phys.* **83**, 1057 (2011).
- [3] N.P. Armitage, E.J. Mele, and A. Vishwanath, Weyl and Dirac semimetals in three-dimensional solids, *Rev. Mod. Phys.* **90**, 015001 (2018).
- [4] H. Okamoto, The Bi-Pt (bismuth-platinum) system, *J. Phase Equilib.* **12**, 207 (1991).
- [5] G. Shipunov, I. Kovalchuk, B.R. Piening, V. Labracherie, A. Veyrat, D. Wolf, A. Lubk, S. Subakti, R. Giraud, J. Dufouleur *et al.*, Polymorphic PtBi₂: Growth, structure, and superconducting properties, *Phys. Rev. Mater.* **4**, 124202 (2020).
- [6] L. Xing, R. Chapai, R. Nepal, and R. Jin, Topological behavior and Zeeman splitting in trigonal PtBi_{2-x} single crystals, *npj Quantum Materials* **5**, 10 (2020).
- [7] V.F. Correa, P. Pedrazzini, D.G. Franco, A.J. Rosa, B. Rubrecht, and N. Haberkorn, Low-temperature thermal expansion of the topological material candidates β -PtBi₂ and β -PdBi₂, *Physica B* **641**, 414102 (2022).
- [8] W. Gao, N. Hao, F. Zheng, W. Ning, M. Wu, X. Zhu, G. Zheng, J. Zhang, J. Lu, H. Zhang *et al.*, Extremely large magnetoresistance in a topological semimetal candidate pyrite PtBi₂, *Phys. Rev. Lett.* **118**, 256601 (2017).
- [9] C.Q. Xu, X.Z. Xing, X. Xu, B. Li, B. Chen, L.Q. Che, X. Lu, J. Dai, and Z.X. Shi, Synthesis, physical properties, and band structure of the layered bismuthide PtBi₂, *Phys. Rev. B* **94**, 165119 (2016).
- [10] L. Zhao, L. Xu, H. Zuo, X. Wu, G. Gao, and Z. Zhu, Fermi surface and carrier compensation of pyrite-type PtBi₂ revealed by quantum oscillations, *Phys. Rev. B* **98**, 085137 (2018).
- [11] W. Gao, X. Zhu, F. Zheng, M. Wu, J. Zhang, C. Xi, P. Zhang, Y. Zhang, N. Hao, W. Ning, and M. Tian, A possible candidate for triply degenerate point fermions in trigonal layered PtBi₂, *Nat. Commun.* **9**, 3249 (2018).
- [12] Y. Wu, N.H. Jo, L. Wang, C.A. Schmidt, K.M. Neilson, B. Schrunck, P. Swatek, A. Eaton, S. L. Bud'ko, P.C. Canfield, and A. Kaminski, Fragility of Fermi arcs in Dirac semimetals, *Phys. Rev. B* **99**, 161113(R) (2019).
- [13] S. Thirupathaiah, Y. Kushnirenko, K. Koepernik, B. R. Piening, B. Büchner, S. Aswartham, J. van den Brink, S. Borisenko, and I. C. Fulga, Sixfold fermion near the Fermi level in cubic PtBi₂, *SciPost Phys.* **10**, 004 (2021).
- [14] X. Yang, H. Bai, Z. Wang, Y. Li, Q. Chen, J. Chen, Y. Li, C. Feng, Y. Zheng, and Z.-A. Xu, Giant linear magnetoresistance in nonmagnetic PtBi₂, *Appl. Phys. Lett.* **108**, 252401 (2016).
- [15] B. Wu, V. Barrena, H. Suderow, and I. Guillamón, Huge linear magnetoresistance due to open orbits in γ -PtBi₂, *Phys. Rev. Res.* **2**, 022042(R) (2020).
- [16] S. Thirupathaiah, Y. Kushnirenko, E. Haubold, A. V. Fedorov, E. D. L. Rienks, T. K. Kim, A. N. Yaresko, C. G. F. Blum, S. Aswartham, B. Büchner, and S. V. Borisenko, Possible origin of linear magnetoresistance: Observation of Dirac surface states in layered PtBi₂, *Phys. Rev. B* **97**, 035133 (2018).
- [17] N.E. Alekseevskii, Yu.P. Gaidukov, Investigations of Bismuth alloys at very low temperatures, *J. Exptl. Theoret. Phys. (U.S.S.R.)* **25**, 383 (1953); N.N. Zhuravlev, L. Kertes, Structure of Superconductors. XI Investigation of Alloys of Bismuth with Platinum, Ruthenium, Osmium and Iridium, *Soviet Phys. JETP* **5**, 1073 (1957).
- [18] A. Veyrat, V. Labracherie, D.L. Bashlakov, F. Caglieris, J.I. Facio, G. Shipunov, T. Charvin, R. Acharya, Y.

- Naidyuk, R. Giraud, J. van den Brink, B. Büchner, C. Hess, S. Aswartham, and J. Dufouleur, Berezinskii-Kosterlitz-Thouless transition in the type I Weyl semimetal PtBi₂, *Nano Lett.* **23**, 1229 (2023).
- [19] X. Chen, D. Shao, C. Gu, Y. Zhou, C. An, Y. Zhou, X. Zhu, T. Chen, M. Tian, J. Sun, and Z. Yang, Pressure-induced multiband superconductivity in pyrite PtBi₂ with perfect electron-hole compensation, *Phys. Rev. Mater.* **2**, 054203 (2018).
- [20] J. Wang, X. Chen, Y. Zhou, C. An, Y. Zhou, C. Gu, M. Tian, and Z. Yang, Pressure-induced superconductivity in trigonal layered PtBi₂ with triply degenerate point fermions, *Phys. Rev. B* **103**, 014507 (2021).
- [21] D.L. Bashlakov, O.E. Kvitnitskaya, G. Shipunov, S. Aswartham, O.D. Feya, D.V. Efremov, B. Büchner, and Yu.G. Naidyuk, Electron-phonon interaction and point contact enhanced superconductivity in trigonal PtBi₂, *Low Temp. Phys.* **48**, 747 (2022).
- [22] S. Schimmel, Y. Fasano, S. Hoffmann, J. Puig, G. Shipunov, D. Baumann, S. Aswartham, B. Büchner, and C. Hess, High- T_c surface superconductivity in topological Weyl semimetal t-PtBi₂, arXiv:2302.08968.
- [23] A. Kuibarov, O. Suvorov, R. Vocaturo, A. Fedorov, R. Lou, L. Merkwitz, V. Voroshnin, J.I. Facio, K. Koepnik, A. Yaresko, G. Shipunov, S. Aswartham, J. van den Brink, B. Büchner, and S. Borisenko, Evidence of superconducting Fermi arcs, *Nature* **626**, 294 (2024).
- [24] See supplemental material at...
- [25] T.T.M. Palstra, B. Batlogg, L.F. Schneemeyer, and J.V. Waszczak, Thermally activated dissipation in Bi_{2.2}Sr₂Ca_{0.8}Cu₂O_{8+ δ} , *Phys. Rev. Lett.* **61**, 1662 (1988).
- [26] C.K. Jones, J.E. Hulm and B.S. Chandrasekhar, Upper critical field of solid solution alloys of the Transition Elements, *Rev. Mod. Phys.* **36**, 74 (1964).
- [27] J.A. Woollam, and R.B. Somoano, Superconducting critical fields of alkali and alkaline-earth intercalates of MoS₂, *Phys. Rev. B* **13**, 3843 (1976).
- [28] D.E. Prober, R.E. Schwall, and M.R. Beasley, Upper critical fields and reduced dimensionality of the superconducting layered compounds, *Phys. Rev. B*, **21**, 2717 (1980).
- [29] Y.J. Jo, J. Jaroszynski, A. Yamamoto, A. Gurevich, S.C. Riggs, G.S. Boebinger, D. Larbalestier, H.H. Wen, N.D. Zhigadlo, S. Katrych *et al.*, High-field phase-diagram of Fe arsenide superconductors, *Physica C* **469**, 566 (2009).
- [30] T.K. Worthington, W. J. Gallagher, and T. R. Dinger, Anisotropic Nature of High-Temperature Superconductivity in Single-Crystal Y₁Ba₂Cu₃O_{7-x}, *Phys. Rev. Lett.* **59**, 1160 (1987).
- [31] Y. Hidaka, M. Oda, M. Suzuki, A. Katsui, T. Murakami, N. Kobayashi, Y. Muto, Anisotropic upper critical magnetic field in single crystal Ba₂YCu₃O_{7-y}, *Physica* **148B**, 329 (1987).
- [32] R.A. Klemm, A. Luther, and M.R. Beasley, Theory of the upper critical field in layered superconductors, *Phys. Rev. B* **12**, 877 (1975).
- [33] A. Gurevich, Enhancement of the upper critical field by nonmagnetic impurities in dirty two-gap superconductors, *Phys. Rev. B* **67**, 184515 (2003).
- [34] J. Hessert, M. Huth, M. Jourdan, H. Adrian, C.T. Rieck, K. Scharnberg, Temperature and angular dependence of the upper critical field of UPd₂Al₃ thin films, *Physica B* **230-232**, 373 (1997).
- [35] C.D. O'Neill, J.L. Schmeh, A.D. Huxley, Multicomponent odd-parity superconductivity in UAu₂ at high pressure, *Proc. Nat. Acad. Sci.* **119**, e2210235119 (2022).
- [36] Y. Nakajima, T. Nakagawa, T. Tamegai, H. Harima, Specific-Heat Evidence for Two-Gap Superconductivity in the Ternary-Iron Silicide Lu₂Fe₃Si₅, *Phys. Rev. Lett.* **100**, 157001 (2008).
- [37] A. Veyrat, Superconductivity and topology in trigonal-PtBi₂, Ph.D. thesis, Technische Universität Dresden 2022.